Composites Science and Technology 213 (2021) 108899

Contents lists available at ScienceDirect

Composites Science and Technology

journal homepage: www.elsevier.com/locate/compscitech

Multi-performance shape memory epoxy resins and their composites with narrow transition temperature range

Lan Luo, Fenghua Zhang, Jinsong Leng *

Centre for Composite Materials and Structures, Harbin Institute of Technology (HIT), Harbin, 150080, PR China

ARTICLE INFO

Keywords:
Shape memory epoxy
Multi-amines
Narrow transition temperature range
Sea-island structure
Two-stage curing

ABSTRACT

Shape memory epoxy resins are one of the most widely used engineering smart polymers, which is mainly used in active deformation structures in aerospace, intelligent bionics, and other fields. A series of shape memory epoxy resins with a narrow glass transition temperature range, strong inter-segment forces and uniform cross-linked networks were designed and synthesized in this study. By adjusting the stoichiometric ratio and cross-linking density, the length of the chain segment was controlled uniformly. The glass transition temperature range reached 14–23 °C, which improved the efficiency of shape memory action. In addition, the multi-amines crosslinking agents were used to adjust the distribution of the chain segment and achieve the effect of regulating the glass transition temperature (Tg). Moreover, the addition of epoxy-terminated liquid nitrile rubber (ETBN) composites enabled toughen of systems. The elongation at break could be increased by 4 times. Furthermore, Tg, modulus and strength of composites were improved by adding high-temperature latent hardener based on the ETBN toughening system combined with two-stage curing method. The composites with narrow transition temperature range were more suitable for shape fixation and recovery temperature with higher precision and closer spacing, which meet the higher requirements in aerospace field.

1. Introduction

In nature, the response of organisms to environmental stimuli is extremely common. For example, chameleon changes color to adapt to the environment, and mimosa leaves slowly close when they encounter rain. In external stimuli such as heat, light, magnetism, electricity, and chemical solvents [1–5], the deformable polymer can memorize temporary shapes that recover to the original shapes in response to stimuli, called shape memory polymers (SMPs). Owing to the characteristics of variable stiffness, variable shape, self-driven, and self-adaption, SMPs have shown wide application prospects in biomedical science, intelligent manufacturing, bionics, engineering and other fields, and have attracted more and more attention [6–9].

Compared with thermoplastic SMPs, thermosetting SMPs has the advantages of high resistance to strain damage, high strength, high modulus, and high storage strain. Among the thermosetting SMPs, epoxy resin (EP) has excellent mechanical properties and fatigue resistance. It can be made into composite materials with continuous fibers, short fibers and other reinforcement materials, which can overcome the shortcomings of insufficient shape resilience for space deployment structures [10–12]. Researchers continue to explore shape memory epoxy (SMEP) by changing the types and proportions of hardeners, resins, and adding various kinds of SMEP composite materials with different functions. Amine hardener is one of the most common epoxy hardeners. However, in the previous reports, the glass transition temperature range of the amine-epoxy system is relatively wide. Ordinary EP with a random cross-linked network structure shows a side-chain space effect. When the shape is fixed or recovered, sufficient heat energy can be obtained in the glass transition region to provide coordinated molecular motion and configuration changes. The glass transition temperature range of common epoxy resins exceeds 60 °C [13–19], and the rigidity can be lost at higher temperatures. However, it is particularly necessary to maintain the rigidity of the material near the glass transition temperature (Tg). The temporary shape needs to be completely fixed at Tg-10 °C, and the original shape must be completely restored at Tg. For example, in the harsh space environment, it is necessary to complete the shaping-unfolding transformation processes at the adjacent temperatures, which requires materials to have high-temperature sensitivity. The smart mold can quickly fix the deformed state for demolding, and the smart information carrier can

* Corresponding author.
E-mail address: lengjs@hit.edu.cn (J. Leng).

https://doi.org/10.1016/j.compscitech.2021.108899
Received 6 October 2020; Received in revised form 21 April 2021; Accepted 30 May 2021
Available online 13 June 2021

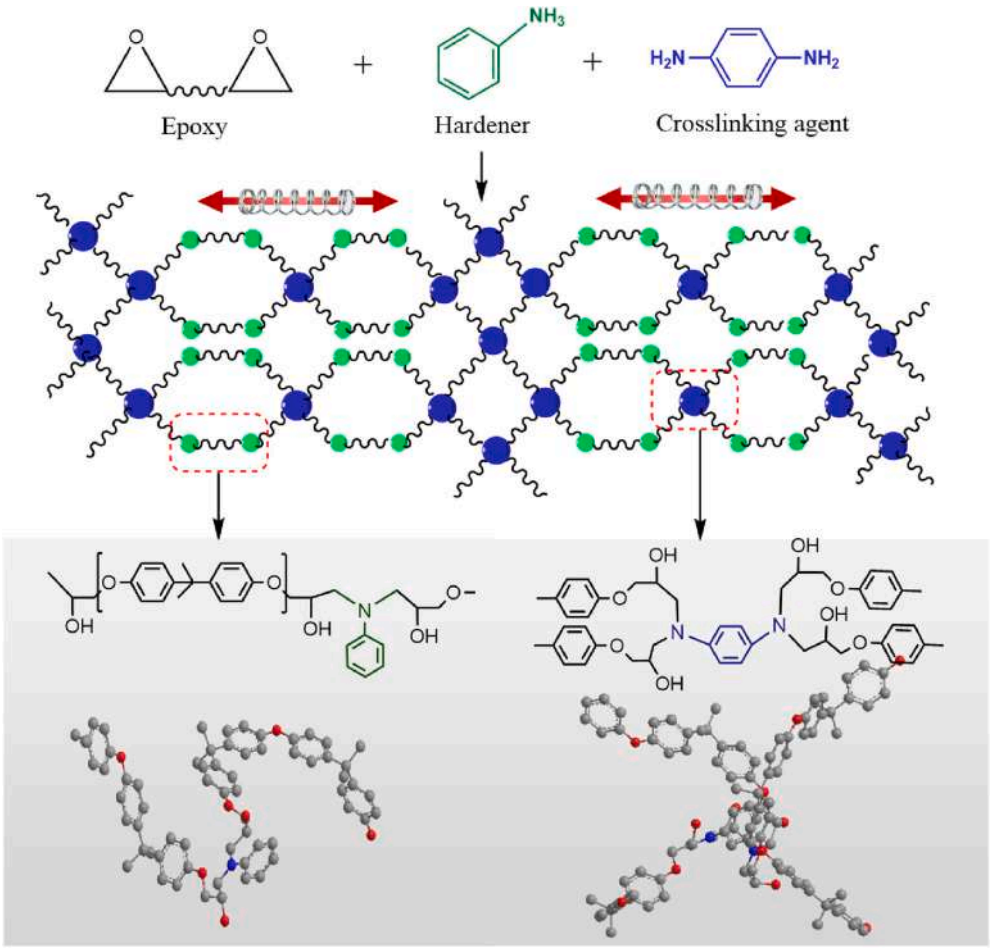

Scheme 1. Schematic illustration of the regular and uniform cross-linked network of SMEP.

quickly record the initial code. However, most SMEPs are unable to complete the entire fixed-recovery process quickly in a narrow temperature range. At present, only shape memory alloys can be realized in a narrow temperature range, such as NiTi alloys [20–22]. There are few studies and reports on the glass transition interval based on SMEP. After curing, SMEP has some shortcomings, such as high internal stress, poor brittleness and heat resistance. The application of the aerospace industry is also limited, and the toughening of SMEPs need to be studied. Currently, toughening technologies of SMEPs mainly include flexible chain toughening, nanoparticle toughening, core-shell structure toughening, thermotropic liquid crystal polymer toughening, interpenetrating network polymer toughening, hyperbranched polymer toughening, etc [23–28]. However, in most aerospace and other applications, it is still a problem to be solved to obtain materials with high Tg and high toughness at the same time [13,29]. The Tg of the system is related to the degree of curing, and the difficulty of chain segment activity requires a higher Tg. Therefore, in order to increase Tg, a two-stage curing method was proposed. Ferracane et al. reported thermal polymerization and photopolymerization, and analyzed the conditions to improve the thermal efficiency and mechanical resistance of the two-stage polymerization technology [30]. Liu et al. studied thermal polymerization and photopolymerization, and analyzed the conditions to improve the thermal performance and mechanical strength of the two-stage polymerization technology [31,32].

Table 1
Formulation of different mixture SMEPs.

	Sample	Ingredient		
System 1		Epoxy/mol%	Aniline/mol%	Multi-amines/mol%
	SMEP-1	60	35	Diamines 5
	SMEP-2	60	35	Triamines 5
	SMEP-3	60	35	Tetramine 5
System 2		Epoxy/mol%	Diamines/mol%	ETBN/mol%
	EP-ETBN$_5$	55	40	5
	EP-ETBN$_{10}$	50	40	10
	EP-ETBN$_{15}$	45	40	15
	EP-ETBN$_{20}$	40	40	20
System 3		EP-Di-/mol%	ETBN/mol%	DICY/mol%
	EP-ETBN$_{10}$	90	10	0
	EP-ETBN$_{10}$*	80	10	10
	EP-ETBN$_{10}$**	80	10	10

*: Add DICY without high-temperature initiation.
**: Add DICY and high-temperature initiation.

In this work, we proposed a series of SMEPs and their composites with a narrow transition temperature range. We selected hardener and crosslinking agents with benzene-rings and obtained a strong and regular network structure by adjusted the ratio of reagents. As shown in Scheme 1, the distribution of chain segments between the crosslinking networks is uniform, and the Tg range of SMEP is reduced. The Tg value could be adjusted by changing the crosslinking agents. Secondly, liquid epoxy-terminated nitrile rubber (ETBN) was added. Compared with other rubbers, the epoxy groups at both ends of ETBN also participated in the crosslinking network, forming a tough composite. Finally, based on ETBN/EP composites, two-stage curing method was selected to improve the internal crosslinking density, mechanical strength and heat resistance.

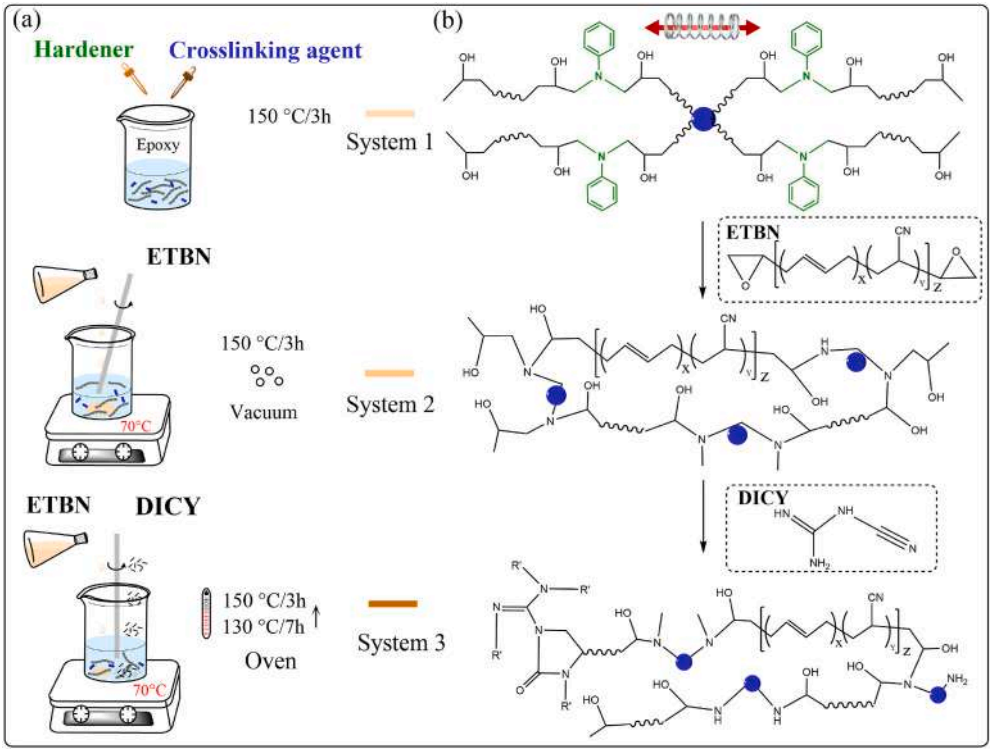

Fig. 1. (a) Preparation process of systems. (b) Reaction process for preparing systems.

2. Experimental

2.1. Materials

The epoxy resin we used was bisphenol A glycidyl ether (DEGBA). Aniline was served as hardener. Diamines (p-Phenylenediamine), triamines (1,3,5-triaminobenzene), and triamines (3,3′-Diaminobenzidine) were used as crosslinking agents. The ratio of hardeners and crosslinking agents plays an important role in uniform distribution of molecular segments caused a narrow glass transition temperature range. Diamines, triamines, and tetramine were used to adjust the value of Tg. The Epoxy-terminated liquid NBR (ETBN) by Suzhou Junxin Plastic Co., China. Dicyandiamide (DICY) (Particle size $\leq$5 μm)was selected as the high-temperature latent hardener in this study by Guangzhou Shinshi Metallurgical and Chemical co., LTD.

2.2. Preparation of system

All the samples of the systems were synthesized using various reagents in different ratios (as shown in Table .1). A series of System 1 was prepared by ultrasonic mixing of different crosslinking agents and monoamines, respectively adding into DEGBA. Based on System 1, different contents of ETBN were added and vacuumed at 60 °C until it was transparent and no bubbles escaped, and the solution was uniform. A series of ETBN/EP composite System 2 was obtained. The curing conditions of Systems 1 and 2 were 100 °C for 2 h and 140 °C for 8 h. A two-stage curing System 3 was prepared by adding DICY in System 2 and curing. To compare the two-stage curing results, we took out a part of the sample (EP-ETBN$_{10}$*) as a control, and continued to heat and cure the remained samples at 180 °C for 3 h. The specific preparation process of all samples is shown in Fig. 1a.

2.3. Characterization methods

2.3.1. Thermal analysis

Fourier transform infrared spectroscopy (FT-IR) tests were performed on a Nicolet-Nexus-670 Fourier transform infrared spectrometer with samples dispersed in KBr particles. The wavelengths from 400 to 4000 cm^{-1} was selected to evaluate the molecular structure of the different epoxy curing systems. The glass transition behavior of samples was studied by differential scanning calorimetry (DSC). Under the nitrogen atmosphere, the samples were scanned by DSC at 5 °C/min from 25 °C to 200 °C. By selecting a second heating cycle (all samples have the same thermal history) to measure the transition temperature, the influence of the material thermal history could be avoided. Thermogravimetric analysis (TGA) performed a thermal stability test. The samples were raised from 25 °C to 800 °C in a ceramic crucible at a rate of 10 °C/min in nitrogen atmosphere.

2.3.2. Static mechanical analysis

The mechanical properties of the samples were evaluated by tensile test. The specimen was dumbbell-shaped with a thickness of 2–3 mm. The tensile test was carried out at room temperature at a tensile speed of 2 mm/min. Then, the fracture morphology was observed by scanning electron microscope (SEM) after sputtering gold plating.

2.3.3. Shape-memory behavior

Dynamic thermomechanical analysis (DMA) investigated the thermo-mechanical properties of the samples. The temperature range was 25 °C–150 °C, and the constant frequency of the applied strain was 1 Hz. Shape memory behavior was tested by bending, stretching, and indentation recovery. After heating them to Tg and molding, the deformed shape was cooled by external force and quickly obtained a temporary shape. Also, to compare the effect before and after toughening, the words "HIT's 100th anniversary" were print on the specimen under the pressure of 0.3 MPa. The shape recovery process and shape recovery ratio were monitored, and the shape recovery degree with time was observed according to the recorded images.

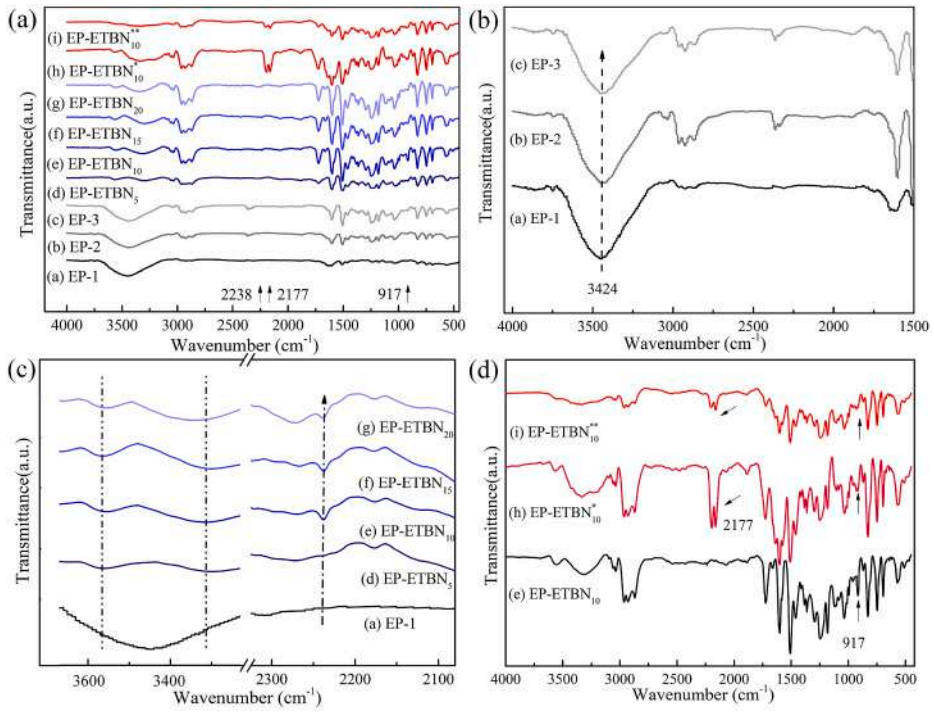

Fig. 2. FTIR spectra of SMEPs: (a) SMEPs. (b), (c) and (d) zoom in part of (a).

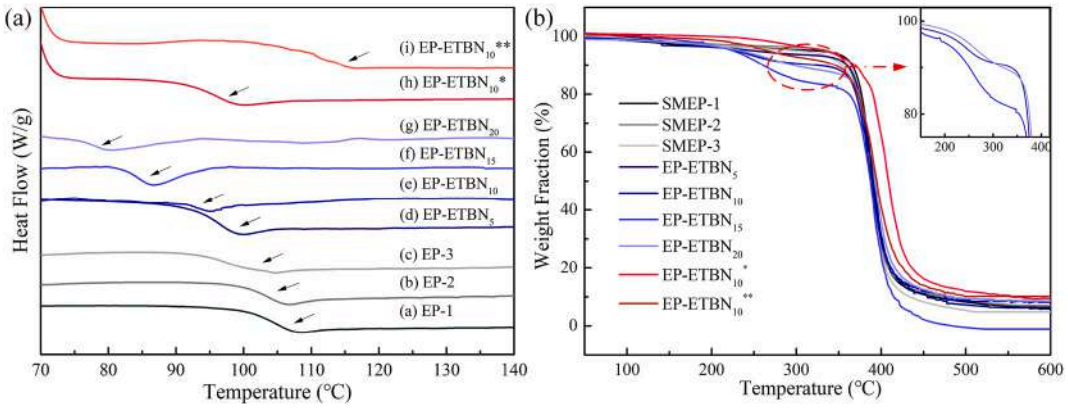

Fig. 3. (a) DSC thermograms of systems. (b) The thermogravimetric curve of the system.

3. Results and discussion

3.1. Material characteristics

The FTIR curves of all samples are shown in Fig. 2a. There was a wide absorption peak of hydroxyl in EP at 3500 cm^{-1}. The tensile vibration strength of the hydroxyl group (O-H) appeared at 3424 cm^{-1}, which decreased with the increase of active hydrogen atoms on the multi-amine cross-linking agents, indicated that the crosslink density also decreased as shown in Fig. 2b. Compared with pure EP, the absorption peak of the cyano group of ETBN/EP composites appeared at 2238 cm^{-1} as shown in Fig. 2c. And as the content increased, the cyano absorption peak became stronger, which indicated that the cyano group was unreactive. The results showed that two peaks appeared at 3600-3300 cm^{-1}, indicated that both ETBN and epoxy groups on the EP participated in the curing reaction. The terminal epoxy group of ETBN was opened under the reaction of hardener and connected with the epoxy group in EP to form a network structure through hardeners. The cross-linked network formed between ETBN and EP improved the compatibility and promoted the toughness of the composites.

The absorption peak of the epoxy group at 917 cm^{-1}gradually disappeared with increased curing degree as shown in Fig. 2d. After the addition of DICY, the absorption peak of cyano stretching vibration in dicyandiamide appeared at 2177 cm^{-1}. The intensity of the absorption peak of EP-$ETBN_{10}$**was significantly weakened after two-stage curing. Meanwhile, the disappearance of the absorption peak of the epoxy group indicated that the curing reaction of dicyandiamide and EP occurred at high temperature. The reaction mechanism is demonstrated in Fig. 1b.

3.2. Thermomechanical behavior

The DSC curves of all samples are shown in Fig. 3a. It can be seen from the curves (a)-(c) that with the increase of active hydrogen in the multi-amines hardener, the Tg of System 2 decreased. The length of the molecular chain segment was shortened and the mobility of the chain end was high, so the network cross-linking and Tg reduced. With the increase of the ETBN content, the Tg of the ETBN/EP composites was directly shifted from the curve (d)-(g) to low temperature. Especially,

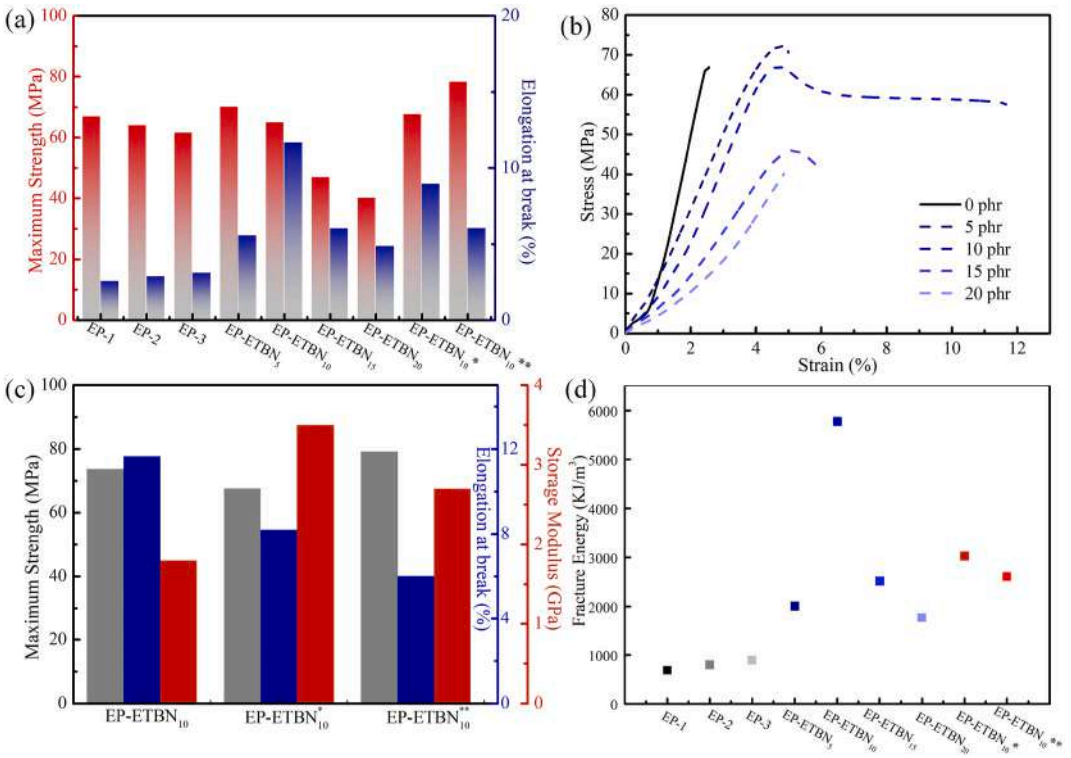

Fig. 4. Mechanical properties of systems: (a) and (b) results of a tensional test at room temperature. (c) typical stress-strain curves at room temperature. (d) toughness at room temperature.

when the ETBN content reached 20 phr, the Tg dropped from 100 °C to 80 °C. According to free volume theory, the increase of molecular chain "occupied volume" of the nitrile rubber led to the change of Tg. The more flexible chains is, the easier the chain moves, and the greater the Tg decreases. It can be seen from the curves (h) and (i) that the Tg decreases about 30 °C before and after the two-stage curing. DICY induced the crosslinking degree increasing, which caused the Tg of EP-ETBN$_{10}$* increased by 10 °C.

The thermal stability of the samples under a nitrogen atmosphere is illustrated in Fig. 3b. Each sample had a degradation stage, which was the weight loss caused by decomposition of the main carbon chain. After adding ETBN, the ETBN/EP composites appeared a step at 200°C–300 °C and the weight loss reached 9.8% as shown in the upper right corner of Fig. 3b. The main decomposition temperature (Td) of pure resin SMEP

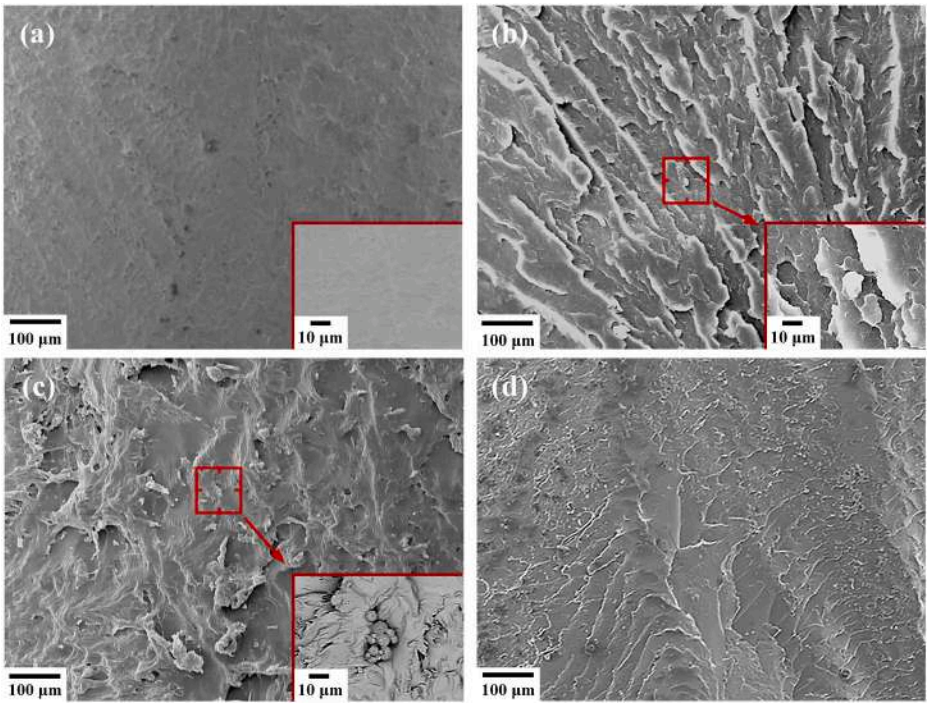

Fig. 5. SEM micrographs of the fracture surface for systems: (a) pure ESMP, (b) EP-ETBN5, (c) EP-ETBN10 and (d) EP-ETBN10**.

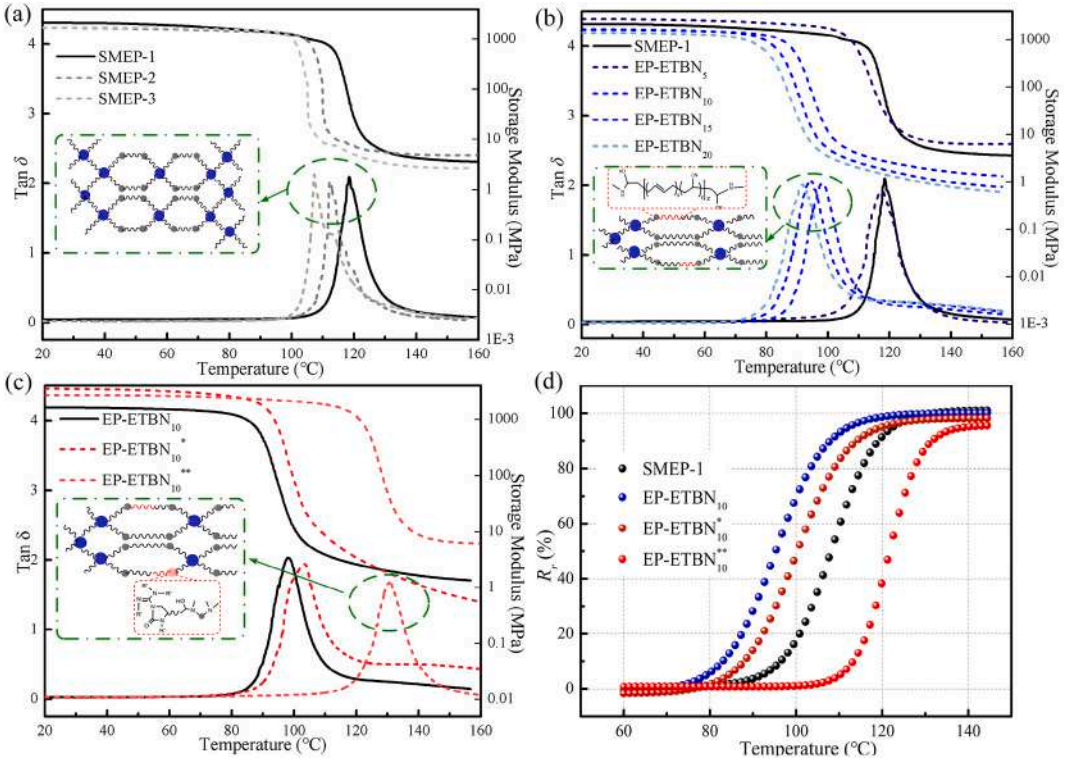

Fig. 6. (a), (b), and (c) The DMA curves of systems. (d) The shape recovery ratio of System 3.

started at 355 °C and the maximum thermal weight loss rate occurred around 385 °C. It has been verified that all samples could be safely handled and used within their Tg range. Besides, the results showed that the thermal stability of the EP-ETBN$_{10}$** composites was slightly improved after two-stage curing, and the decomposition temperature was significantly higher than that before high-temperature curing.

3.3. Static mechanical properties

Tensile testing is usually used to evaluate the static mechanical properties of materials. The strength gradually decreases, and the elongation gradually increases as shown in Fig. 4a. Compared with EP-ETBN$_{10}$, the strength improved to 78 MPa after two-stage curing. When the ETBN content increased from 0 phr to 20 phr, the higher the precipitation density of rubber phase was, the lower the strength was. The strength of EP-ETBN$_5$ reached 70 MPa, which was about 7 MPa higher than that before toughening. When the content was 10 phr, without sacrificing the strength and the elongation at break reached 11.7%, which was increased by more than 4 times as shown in Fig. 4b. When the rubber content increased, the elongation at break decreased due to the incomplete phase separation between ETBN and EP. Moreover, the entanglement of the rubber flexible segments with the resin chain ends causes the blocking of the segments [33]. The elongation at break of EP-ETBN$_{10}$* without two-stage curing was almost not sacrificed. Although the elongation of System 3 reduced, it was still ductile fracture. After the two-stage curing, the modulus also increases significantly as shown in Fig. 4c. Especially, in the absence of high-temperature initiation, due to the crystallization of DICY particles, the strengthening modulus is 3.5 GPa, which is decreased by 0.8 GPa after high-temperature curing. The results showed that high temperature curing can effectively improve the mechanical properties of ETBN/EP composites. The toughness of the material is indirectly evaluated by the area of the strain-stress curve, as shown in Fig. 4d. After two-stage curing, the toughness of ETBN/EP composites decreased, but it was better than that of SMEP.

The fracture surface of pure epoxy resin is smooth and the crack is sharp strip, as shown in Fig. 5a, which belongs to the typical brittle fracture. After adding ETBN, the rubber phase gradually precipitates, forming small spheres dispersed in the resin matrix to form a “sea-island structure”, as shown in Fig. 5b–d. When the ETBN content increased from 5 phr to 15 phr, the rubber particle size increased. As the ETBN continued to increase to 20 phr, the rubber particles in the composites became larger and agglomerates, leading to the strength decreased. When the rubber particles were encountered and the micropores were formed around them, the cracks stopped. As shown in Fig. 5c, the fracture toughness at the crack tip is reduced. The tensile fracture sections of EP-ETBN$_{10}$** are shown in Fig. 5d. The cross-section was staggered, and the silver fringe appeared at the fracture of the stress stripes. It indirectly indicated that after two-stage curing, the energy absorbed by the cracks was a part of the tensile energy, and composites were ductile fracture.

3.4. Shape memory properties

The prepared multi-amine epoxy and their composites have excellent shape memory performance as shown in Fig. 6 and Table S1(Supporting Information). Dynamic thermomechanical test showed the thermodynamic properties of the shape memory polymer. Tg can also be obtained from the peak of the loss factor in the DMA curve, and the change trend was similar to DSC (Fig. 3a). The decrease of Tg values of the toughening system in DMA was due to the addition of ETBN.

With the increases of active hydrogen content in multi-amine hardeners, Tg of the system decreased. Fig. 6a outlines that the range of glass transition temperature is relatively narrow around 20 °C. Compared with ordinary EP [34], the thermal deformation temperature range was shortened, and the rapid setting was achieved. Similar to NiTi shape memory alloy, it can achieve a narrower temperature transition [21]. The main reason was that the benzene ring in the chain made the molecular chain have π-π interaction, which made the force between the chain segments stronger. On the other hand, different chain segments

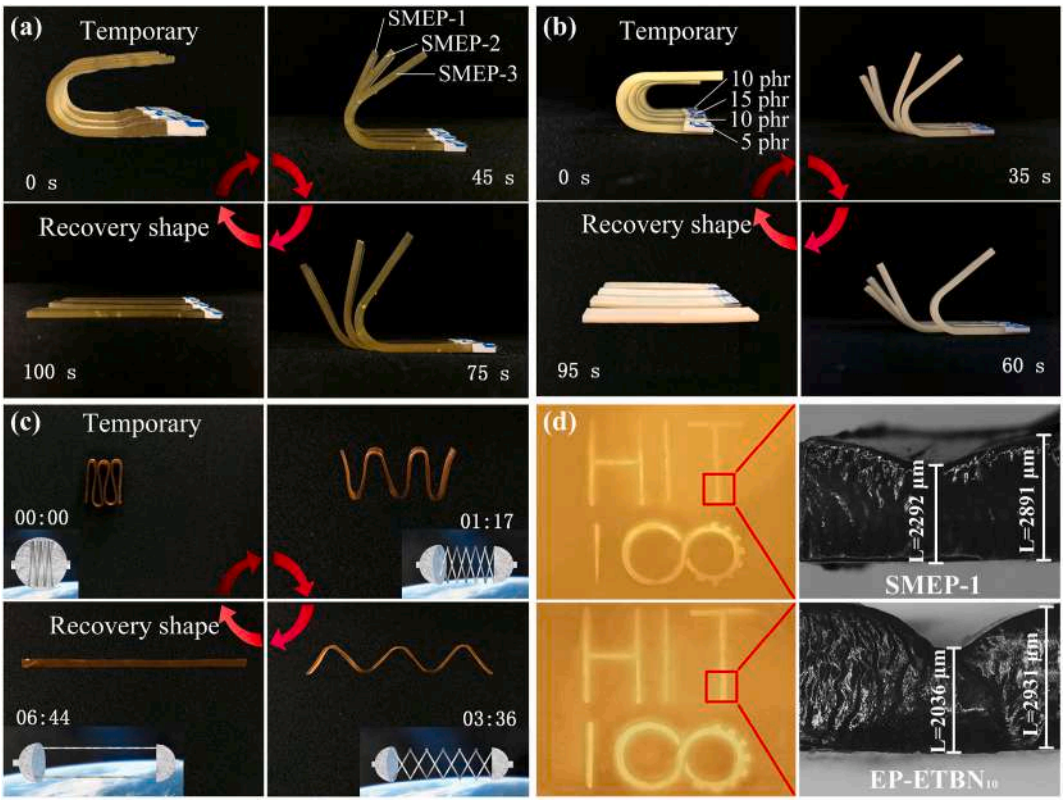

Fig. 7. Characterization of the shape-memory behavior of systems: (a) and (b) Shape recovery process, (c) Simulation process of space capsule, (d) Engrave "the 100th Anniversary".

have their own motion temperatures, and different motion temperature distributions show the glass transition range. The uniform chain length and regular network structure shortened the temperature range of the whole chain. When the epoxy group was constant, Tg decreased with the increase of active hydrogen content and branch chain number. With the increases of ETBN content, Tg decreased gradually. In Fig. 6b, the peak width of ETBN slightly increases by 2–3 °C. Since the epoxy group in ETBN also participated in the reaction, the molecular segment changed. Compared with EP-ETBN$_{10}$, Tg of the composites increases by more than 30 °C, and the magnitude difference of modulus decreases after two-stage curing, as shown in Fig. 6c. The load capacity of the composites increased with the increase of strength and modulus after two-stage curing. Two-stage curing was to improve the curing degree and cross-linking degree of the system. The increase of cross-linking points led to the decrease of tan δ. The results showed that the relative displacement of the molecular segment motion decreased and the internal friction became smaller. DICY was not initiated by high temperature and dissolved in SMEP to form precipitate crystals, which could greatly improve the modulus of EP-ETBN $_{10}$*. After two-stage curing at high temperature, the modulus of EP-ETBN$_{10}$** in the glass transition process only decreased by less than 2 orders of magnitude, and the modulus also increased. Similarly, Tang et al. [35,36] studied that the modulus in DMA curve decreased by at least 2 orders of magnitude, indicating that SMP has excellent shape memory effect.

It is worth mentioning that all samples can be shaped and recovered quickly. For example, SMEP-1 could completely fix the shape at 105 °C, fully recover at 120 °C, and even slowly recover at 115 °C, which improved the efficiency of shape memory. The shape fixing temperature and shape recovery temperature could be precisely controlled to meet the higher requirements of aerospace field. As the temperature gradually rose, the free volume of the segment increased and the thermal motion of the molecule accelerated. With the release of internal stress, the initial rapid release of molecules and molecular segments decreased. Finally, the internal stress was almost exhausted and recovered slowly. The two-stage cured samples of System 3 were heated gradually from 60 °C and recorded every 10 min until the shape was completely recovered. Boltzmann Fit was used to fit the S-curve fitting of the tested data. Fig. 6d shows the recovery curve after fitting. After two-stage curing, the recovery ratio of EP-ETBN$_{10}$** decreased slightly, which was due to the deepening of the cross-linking degree caused by two-stage curing. In addition, DICY hindered the movement of the chain segments in the system, leading to a decrease in shape recovery ratio as shown in Table S1(Supporting Information).

Both Systems 1 and 2 showed excellent shape memory performance. As shown in Fig. 7a, the multi-amine epoxy resin samples were simultaneously recovered at Tg+20 °C. The decrease of crosslinking degree led to a relatively small resistance to fragment movement. With the increase of active hydrogen content, the deformation recovery ability increased. The higher the recovery ratio was, the shorter the recovery time was. After adding the rubber phase, the higher the ETBN content was, the faster the recovery was (as shown in Fig. 7b). This means that ETBN increased the number of internal motion chain segments in the system. During shape memory programming, the composite was stretched to the specified maximum stress, which corresponded to 75% of the fracture stress as shown in Fig. S1(Supporting Information). The multi-folding and deployment through the space capsule deployment experiment are shown in Fig. 7c. EP-ETBN$_{10}$ and SMEP-1 were selected for indentation test as shown in Fig. 7d. The samples with "HIT's 100th Anniversary" were tested under the pressure of 0.3 MPa at Tg. The results showed that the change ratios of drop height before and after toughening were 30.53% and 20.17% respectively, and the toughened samples showed excellent elasticity.

In the DMA curve, the glass transition range is the temperature difference between Ts (the temperature at which the modulus decreases) and Tr (the temperature at which the modulus stabilizes). The regular and uniform cross-linking network and the strong inter-segment forces

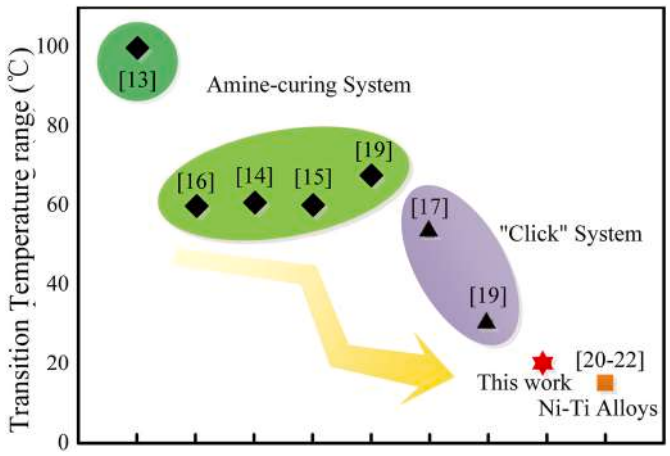

Fig. 8. Comparison of transition temperature range with other literatures.

in the network showed a narrower transition temperature range, which was marked as a Red Hexagram. The performance of SMEP was compared with that reported in other literatures [13–19,21], as shown in Fig. 8. The results showed that the glass transition temperature of common epoxy resin was generally above 60 °C, and the "click reaction" could be shortened to about 40 °C, and our work can reach 14–23 °C.

4. Conclusions

In this work, we describe a series of shape memory epoxy resins and their composites with multi-performance and narrow transition temperature ranges. It was achieved by designing a network structure with strong force between chain segments and uniform chain segment distribution. Different multi-amine curing agents could change Tg by adjusting the crosslinking density to keep it in a narrow transition temperature range of 14–23 °C and keep its rigidity at a higher temperature. In addition, ETBN was added into the system to improve the toughness and then combined with two-stage curing to improve the strength and Tg. SEM results showed that the micro-phase separation occurred during the curing process of the composites with rubber, forming a "sea-island" structure. When the content reached 10 phr, the elongation at break of the composites increased by 4 times and the strength also be improved. Then, two-stage curing was performed on the toughened system by adding a high-temperature latent hardener. After two-stage curing, the tensile strength and heat resistance of the composites were increased by 30 °C and 15 MPa, respectively. The addition of high-temperature hardener improved both the strength and modulus of the composites. In the future, SMEPs and their composites in this work with narrow glass transition temperature ranges may be used as a suitable candidate for aerospace.

Author statement

Lan Luo: Methodology, Writing – original draft. Fenghua Zhang: Data curation, Writing – review & editing. Funding acquisition. Jinsong Leng: Supervision, Funding acquisition.

Declaration of competing interest

The authors declare that they have no known competing financial interests or personal relationships that could have appeared to influence the work reported in this paper.

Acknowledgments

This work is supported by the National Natural Science Foundation of China (No.11632005).

Appendix A. Supplementary data

Supplementary data to this article can be found online at https://doi.org/10.1016/j.compscitech.2021.108899.

References

[1] Q. Zhao, H.J. Qi, T. Xie, Recent progress in shape memory polymer: new behavior, enabling materials, and mechanistic understanding, Prog. Polym. Sci. 49–50 (2015) 79–120.
[2] J. Leng, L. Xin, Y. Liu, S. Du, Shape-memory polymers and their composites: stimulus methods and applications, Prog. Mater. Sci. 56 (7) (2011) 1077–1135.
[3] C. Liu, H. Qin, P.T. Mather, Review of progress in shape-memory polymers, J. Mater. Chem. 17 (16) (2007).
[4] W.M. Huang, B. Yang, Y. Zhao, Z. Ding, Thermo-moisture responsive polyurethane shape-memory polymer and composites: a review, J. Mater. Chem. 20 (17) (2010) 3367–3381.
[5] A. Lendlein, H.Y. Jiang, O. Junger, R. Langer, Light-induced shape-memory polymers, Nature 434 (7035) (2005) 879–882.
[6] C. Lin, J. Lv, Y. Li, F. Zhang, J. Li, Y. Liu, L. Liu, J. Leng, 4D-Printed biodegradable and remotely controllable shape memory occlusion devices, Adv. Funct. Mater. 29 (51) (2019).
[7] A. Lendlein, R. Langer, Biodegradable, elastic shape-memory polymers for potential biomedical applications, Science 296 (5573) (2002) 1673–1676.
[8] T. Mu, L. Liu, X. Lan, Y. Liu, J. Leng, Shape memory polymers for composites, Compos. Sci. Technol. (2018), S0266353817310990.
[9] J. He, Y. Fan, C. Xiao, F. Liu, H. Sun, Z. Zhu, W. Liang, A. Li, Enhanced solar steam generation of hydrogel composite with aligned channel and shape memory behavior, Compos. Sci. Technol. 204 (2021).
[10] F. Li, L. Liu, X. Lan, C. Pan, Y. Liu, J. Leng, Q. Xie, Ground and geostationary orbital qualification of a sunlight-stimulated substrate based on shape memory polymer composite, Smart Mater. Struct. 28 (7) (2019).
[11] Z. Liu, Q. Li, W. Bian, X. Lan, Y. Liu, J. Leng, Preliminary test and analysis of an ultralight lenticular tube based on shape memory polymer composites, Compos. Struct. 223 (2019).
[12] D. Thanh Duc, H. Ngoc San, N.S. Goo, W.-R. Yu, Design, fabrication, and bending test of shape memory polymer composite hinges for space deployable structures, J. Intell. Mater. Syst. Struct. 29 (8) (2018) 1560–1574.
[13] O. Konuray, A. Garcia, J.M. Morancho, X. Fernandez-Francos, A. Serra, F. Ferrando, M. Garcia-Alvarez, X. Ramis, Hard epoxy thermosets obtained via two sequential epoxy-amine condensations, Eur. Polym. 116 (2019) 222–231.
[14] I.A. Rousseau, T. Xie, Shape memory epoxy: composition, structure, properties and shape memory performances, J. Mater. Chem. 20 (17) (2010) 3431–3441.
[15] Y.Y. Liu, C.M. Han, H.F. Tan, X.W. Du, Organic-montmorillonite modified shape memory epoxy composite, Polym. Adv. Technol. 22 (12) (2011) 2017–2021.
[16] R. Ren, Z.P. Zhang, X.H. Xiong, L. Zhou, X.C. Guo, P. Chen, The effect of phthalide cardo structure on the shape memory performance of high-temperature resistant epoxy resins, Mater. Res. Express 5 (11) (2018) 10.
[17] A. Belmonte, X. Fernandez-Francos, S. De la Flor, A. Serra, Network structure dependence on unconstrained isothermal-recovery processes for shape-memory thiol-epoxy "click" systems, Mech. Time-Depend. Mater. 21 (2) (2017) 133–149.
[18] M.J. Jo, H. Choi, G.H. Kim, W.R. Yu, M. Park, Y. Kim, J.K. Park, J.H. Youk, Preparation of epoxy shape memory polymers for deployable space structures using flexible diamines, Fiber. Polym. 19 (9) (2018) 1799–1805.
[19] Q. Zou, L.H. Ba, X.C. Tan, M.J. Tu, J. Cheng, J.Y. Zhang, Tunable shape memory properties of rigid-flexible epoxy networks, J. Mater. Sci. 51 (23) (2016) 10596–10607.
[20] C. Yang, W. Ye, Y. Ding, S. Feng, Preparation of Narrow-Temperature Zone Controlled-Temperature Nickel-Titanium Shape Memory Alloy Used for Water Heating and Bathroom Industry by Performing Heat Treatment of Untreated Shape Memory Alloy, and Quenching Using Liquid Nitrogen, Univ South China Technology; Kaiping Falanduo Sanitary Ware Co Ltd, 2017.
[21] V.I. Nikolaev, S.I. Stepanov, P.N. Yakushev, V.M. Krymov, S.B. Kustov, Burst-like shape recovery and caloric effects in Ni-Fe-Ga-Co single crystalline shape memory alloys, Intermetallics 119 (2020).
[22] B.S. Shariat, Y. Liu, S. Bakhtiari, Modelling and experimental investigation of geometrically graded shape memory alloys with parallel design configuration, J. Alloys Compd. 791 (2019) 711–721.
[23] M. Fan, J. Liu, X. Li, J. Zhang, J. Cheng, Thermal, mechanical and shape memory properties of an intrinsically toughened epoxy/anhydride system, J. Polym. Res. 21 (3) (2014).
[24] C. Huang, J. Peng, Y. Cheng, Q. Zhao, Y. Du, S. Dou, A.P. Tomsia, H.D. Wagner, L. Jiang, Q. Cheng, Ultratough nacre-inspired epoxy-graphene composites with shape memory properties, J. Mater. Chem. A. 7 (6) (2019) 2787–2794.
[25] T. Ashida, M. Ochi, Structure and adhesive properties of epoxy resins modified with acrylic particles, J. Adhes. Sci. Technol. 11 (4) (1997) 519–530.
[26] J. Yu, W. Hao, A molecular dynamics investigation on evaporation of thin liquid films, Int. J. Heat Mass Tran. 55 (4) (2012) 1218–1225.
[27] Z. Gao, Y. Yu, Y. Xu, S. Li, Synthesis and characterization of a liquid crystalline epoxy containing azomethine mesogen for modification of epoxy resin, J. Appl. Polym. Sci. 105 (4) (2007) 1861–1868.

[28] C. Wang, Y. Zhang, J. Li, Z. Yang, Q. Wang, T. Wang, S. Li, S. Chen, X. Zhang, Shape memory properties of interpenetrating polymer networks (IPNs) based on hyperbranched polyurethane (HBPU), Eur. Polym. J. 123 (2020).
[29] G. Zhou, W. Wang, M. Peng, Molecular-level dispersion of rigid-rod sulfonated aromatic polyamides in epoxy resin for extraordinary improvement in both strength and toughness, Polymer 163 (2019) 20–28.
[30] J.L. Ferracane, J.R. Condon, Postcure heat-treatments for composites - properties and fractography, Dent. Mater. 8 (5–6) (1992) 290–295.
[31] H. Sun, Y. Liu, H. Tan, X. Du, A new method to improve the stability, tensile strength, and heat resistant properties of shape-memory epoxy resins: two-stages curing, J. Appl. Polym. Sci. 131 (4) (2014).
[32] H. Sun, Y. Liu, Y. Wang, H. Tan, Curing behavior of epoxy resins in two-stage curing process by non-isothermal differential scanning calorimetry kinetics method, J. Appl. Polym. Sci. 131 (17) (2014).
[33] K. Mimura, H. Ito, H. Fujioka, Toughening of epoxy resin modified with in situ polymerized thermoplastic polymers, Polymer 42 (22) (2001) 9223–9233.
[34] J. Leng, X. Wu, Y. Liu, Effect of a linear monomer on the thermomechanical properties of epoxy shape-memory polymer, Smart Mater. Struct. 18 (9) (2009).
[35] J.R. Lin, L.W. Chen, The mechanical-viscoelastic model and WLF relationship in shape memorized linear ether-type polyurethanes, J. Polym. Res. 6 (1) (1999) 35–40.
[36] L. Tang, Y. Wang, T. Zhou, Y. Li, Q. Li, Enhanced toughness and mechanical property of epoxy resins with good shape memory behaviors, Fiber. Polym. 21 (6) (2020) 1187–1194.